**PASJ:** Publ. Astron. Soc. Japan **60**, 1057–1067, 2008 October 25


# A Bipolar Outflow of the M-Type Giant IRC −10414 Traced by $H_2O$ Maser Emission

Toshihisa MAEDA,[1] Hiroshi IMAI,[1,2] Toshihiro OMODAKA,[1,2] Hideyuki KOBAYASHI,[3,6,7] Katsunori M. SHIBATA,[3,6,7] Takeshi BUSHIMATA,[3,4] Yoon Kyung CHOI,[3,5] Tomoya HIROTA,[3] Mareki HONMA,[3,6] Koji HORIAI,[7] Noritomo INOMATA,[1] Kenzaburo IWADATE,[3,7] Takaaki JIKE,[3,7] Seiji KAMENO,[1,2] Osamu KAMEYA,[3,6,7] Ryuichi KAMOHARA,[3] Yukitoshi KAN-YA,[3,8] Noriyuki KAWAGUCHI,[3,6,7] Seisuke KUJI,[3,7] Tomoharu KURAYAMA,[3,7] Seiji MANABE,[3,6,7] Takeshi MIYAJI,[3,7] Takumi NAGAYAMA,[1] Akiharu NAKAGAWA,[2] Kouichiro NAKASHIMA,[1] Chung Sik OH,[3,5] Tomoaki OYAMA,[3,7] Satoshi SAKAI,[3,7] Seiichiro SAKAKIBARA,[1] Katsuhisa SATO,[3,7] Rie SHIMIZU,[1] Motonobu SHINTANI,[1] Kasumi SORA,[1] Hiroshi SUDA,[3,7] Yoshiaki TAMURA,[3,6,7] and Kazuyoshi YAMASHITA[3,6]

[1]*Graduate School of Science and Engineering, Kagoshima University, 1-21-35 Korimoto, Kagoshima 890-0065*
[2]*Department of Physics, Faculty of Science, Kagoshima University, 1-21-35 Korimoto, Kagoshima 890-0065*
[3]*Mizusawa VERA Observatory, Mitaka Office, National Astronomical Observatory of Japan, 2-21-1 Osawa, Mitaka, Tokyo 181-8588*
[4]*Space VLBI Project, National Astronomical Observatory, 2-21-1 Osawa, Mitaka, Tokyo 181-8588*
[5]*Department of Astronomy, The University of Tokyo, 7-3-1 Hongo, Bunkyo-ku, Tokyo 113-8654*
[6]*Graduate University for Advanced Studies, 2-21-1 Osawa, Mitaka, Tokyo 181-8588*
[7]*Mizusawa VERA Observatory, National Astronomical Observatory of Japan, 2-12 Hoshigaoka, Mizusawa-Ku, Oshu-shi, Iwate 023-0861*
[8]*Department of Astronomy, Yonsei University, 134 Shinchong-dong, Seodaemun-gu, Seoul 120-749, Republic of Korea*
*maeda, imai@astro.sci.kagoshima-u.ac.jp*

(Received 2008 February 23; accepted 2008 June 4)

**Abstract**

We report on results of five-epoch VLBI observations of $H_2O$ maser emission in the M-type star IRC −10414, carried out with the VLBI Exploration of Radio Astrometry (VERA). The maser distribution extends over an area of 70 mas × 260 mas and exhibits a bipolar structure. The relative proper motions of 17 maser features were measured during the monitoring observations spanning nine months. The distance to IRC −10414 was re-estimated on the basis of the statistical treatment of parallax and the model-fitting method, yielding $D = 3.1 \pm 0.4$ kpc and $D = 2.0 \pm 0.2$ kpc, respectively. The estimated distance, $D = 2$–3 kpc, is much larger than that previously adopted. The stellar luminosity of IRC −10414 is also re-estimated to be $L_* \sim 9 \times 10^4\,(D/2\,\mathrm{kpc})^2 L_\odot$, much brighter by a factor of 10–20 than previously adopted ($L_* \sim 10000\,L_\odot$). The maser motions exhibit not only a spherically expanding flow with a velocity of $\sim 10\,(D/2\,\mathrm{kpc})\,\mathrm{km\,s^{-1}}$, but also a faster bipolar outflow with a major axis in the north–south direction and at a small inclination angle with respect to the celestial sphere. These characteristics of the star and the circumstellar envelope seen in IRC −10414 are very similar to those in some supergiants exhibiting bipolar stellar mass loss.

**Key words:** masers — stars: AGB and post-AGB — stars: individual (IRC −10414) — stars: late-type

## 1. Introduction

A low-mass or intermediate-mass star becomes a white dwarf with a planetary nebula (PN) through the asymptotic giant branch (AGB) phase, in which it undergoes the most copious mass loss in its evolutionary path. There still exists a missing link between the AGB and post-AGB phases in the mass loss history. It has been stated that many young PNe exhibit bipolar morphologies or large deviations from spherical symmetry, while the parent star is assumed to be spherically symmetric (e.g., Aaquist & Kwok 1991; Sahai & Trauger 1998). Such PN asymmetry may be caused by an asymmetric mass-loss process on the stellar surface, which cannot be directly observed because the central stars are heavily obscured by gas and dust ejected from the stars, themselves.

Many AGB stars often exhibit $H_2O$ maser emission consisting of many compact maser features, whose proper motions are measurable with high angular resolution, achieved by very long baseline interferometry (VLBI). The maser emission occurs at distances of between $10^{13}$ m and $10^{14}$ m from the central star; the distribution radius systematically increases with the mass-loss rate (Cooke & Elitzur 1985). The structures of circumstellar envelopes in the $H_2O$ maser regions are clumpy and frequently deviate from spherical symmetry, but the origin of the asymmetry is still unknown. However, some of the maser spatio-kinematical structures of AGB stars clearly indicate the existence of highly collimated bipolar outflows earlier than previously thought (e.g., Imai et al. 2002). The flow collimation mechanism is still unknown, even if the flow collimation is strongly expected to be controlled magneto-hydrodynamically (Vlemmings et al. 2006). There are some theoretical studies that reproduce highly collimated stellar jets from either a single AGB star or a binary system (e.g., Nordhaus & Blackman 2007).

In the present paper, we present maps of $H_2O$ maser emission in IRC −10414, obtained with the VLBI Exploration of Radio Astrometry (VERA) at five epochs. IRC −10414 (AFGL 2139, OH 17.55−0.13, IRAS 18204−1344) is classified as an M8 giant (Lockwood 1985) and a source of bright OH, $H_2O$, and SiO maser emission (Engels 1979; Ukita & Goldsmith 1984). The mass-loss rate of this star was estimated to be $4 \times 10^{-6}\,M_\odot\,\mathrm{yr}^{-1}$ from the infrared spectrum (Jura & Kleinmann 1989). $H_2O$ maser emission in IRC −10414 was found by Kleinman, Dickinson, and Sargent (1978), and mapped with a single baseline (NRAO 43 m–Haystack Observatory 37 m antenna) VLBI by Lada et al. (1981); the latter found four maser features located within 0.″3. The SiO maser emission was mapped by Imai, Deguchi, and Miyoshi (1999, hereafter abbreviated as IDM99) and exhibited a ring structure with a major axis length of $\sim$ 14 mas. Interestingly, the $H_2O$ maser distribution was roughly elongated in the north–south direction, while the SiO maser distribution was perpendicularly elongated. It is expected that a bipolar outflow has just been launched in IRC −10414, which is traced by $H_2O$ maser emission.

Section 2 describes the VERA observations and data reduction. Section 3 presents the $H_2O$ maser spatio-kinematics and an estimation of the distance to IRC −10414 on the basis of statistical parallax and model fitting methods. Section 4 discusses the bipolar outflow found in the $H_2O$ spatio-kinematical structure and the property of the central star.

## 2. Observations and Data Reduction

VERA observations of the IRC −10414 masers were performed at 6 epochs between 2004 July and 2005 April with a typical epoch separation of 1–2 months. Table 1 summarizes the present VERA observations. The observations were made in the dual-beam mode, but only the target maser source and clock parameter calibrators with large anglular distances from the target, NRAO 530 and ICRF J192559.6+210626, were detected. Thus, it was impossible to estimate the absolute coordinates of the maser source through dual-beam astrometry. Left-hand circular polarization signals were digitized in four level quantization, filtered into two base band channels with a band width of 16 MHz (corresponding to a radial velocity span of 215.7 km s$^{-1}$) each, and recorded using the VSOP-terminal at a rate of 128 Mbit s$^{-1}$. The recorded signals were correlated with the Mitaka FX correlator to obtain visibility data with 1024 spectral channels, yielding frequency and velocity resolutions of 7.8 kHz and 0.21 km s$^{-1}$, respectively. The system noise temperatures at the zenith were typically 200 K to 300 K.

In the data analysis of each epoch, a visibility calibration was carried out in a standard manner using the Astronomical Image Processing System (AIPS) of the National Radio Astronomy Observatory (NRAO). The clock parameters (clock offset and clock rate offsets) were calibrated using the residual delays and delay rates of the bright calibrator sources. A bandpass amplitude calibration was performed using auto-correlation spectra of the same continuum sources. The amplitude calibration was made using the system noise temperatures, which were evaluated by observing a radio absorber at room temperature at the beginning of each scan. The observed frequencies of the maser lines were converted to the local-standard of rest (LSR) velocities using a rest frequency of 22.235080 GHz for the $H_2O$ $6_{16}$–$5_{23}$ transition. For the final phase calibration, the visibilities of all velocity channels were phase-referenced to those in the phase-reference velocity channel, whose LSR velocity is given in column 4 in table 1. In the reference channel, one of the brightest maser spots (velocity components) was detected at all epochs, and did not indicate any deviation from the zero closure phases or any complicated brightness structure.

After those processes, the calibrated visibilities were Fourier transformed to a synthesized image. The synthesized beam typically had an FWHM size of 2 mas × 1 mas with a position angle of −20°. The position of a maser feature, a cluster of maser spots distributed in almost the same velocity and location, was determined from the position of the brightest maser spot in the feature and measured with respect to the reference maser spot mentioned above.

## 3. Results

### 3.1. The Spatio-Kinematics of the IRC −10414 $H_2O$ Masers

Figure 1 shows the time variation of the total-power spectrum of $H_2O$ maser emission observed in IRC −10414 from 2004 May to 2005 April. The LSR velocities of the masers ranged from 29 km s$^{-1}$ to 56 km s$^{-1}$, while previous single-dish observations found maser lines ranging from 29 km s$^{-1}$ to 45 km s$^{-1}$ (Kleinman et al. 1978). The systemic (stellar) velocity of IRC −10414 is estimated to be 43.2 km s$^{-1}$ from the OH 1612 MHz double peaks (Blommaert et al. 1994), 37 km s$^{-1}$ from the SiO maser spectrum (Ukita & Goldsmith 1984), 42.2 km s$^{-1}$ from the intensity-weighted velocity of SiO maser spectrum (IDM99), and 34.1 km s$^{-1}$ from the kinematical structure of SiO masers (IDM99). The intensity-averaged LSR velocity of $H_2O$ masers in the present paper is 42.5 km s$^{-1}$, which is approximately in the middle of the velocity range of maser emission and systemic velocities estimated by Blommaert, van Langevelde, and Michiels (1994)

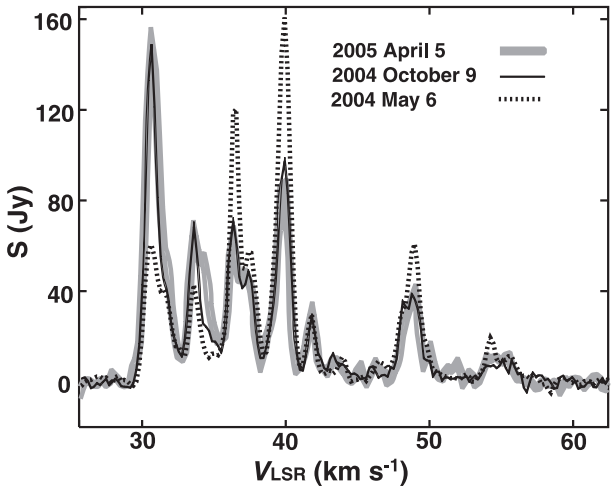


**Fig. 1.** Total-power spectrum of the IRC −10414 $H_2O$ maser emission at the three epochs.

**Table 1.** Status of the telescopes, data reduction, and resulting performances in the individual epochs of the VERA observations.

| Observation code | Observation epoch (YY/MM/DD) | Duration (hr) | Reference velocity* (km s$^{-1}$) | 1-$\sigma$ level noise (Jy beam$^{-1}$) | Synthesized beam† (mas$^2$) | Number of detected features |
|---|---|---|---|---|---|---|
| r04209a | 04/07/27 | 0.9‡ | 36.40 | 4.1 | $6.5 \times 3.1, -26°$ | 9 |
| r04260a | 04/09/15 | 5.7 | 36.46 | 2.5 | $1.8 \times 0.7, -30°$ | 7 |
| r04329b§ | 04/11/24 | 3.5 | ... | ... | ... | ... |
| r04356a | 04/12/21 | 3.5 | 33.59 | 1.4 | $3.4 \times 1.6, -23°$ | 20 |
| r05044a | 05/02/13 | 4.3 | 33.56 | 1.0 | $1.7 \times 0.8, -15°$ | 19 |
| r05104b | 05/04/14 | 4.3 | 33.60 | 1.4 | $1.6 \times 0.8, -25°$ | 32 |

* Velocity channel used for the phase reference in data reduction.
† The synthesized beam made in natural weight; major and minor axis lengths and a position angle.
‡ Snapshot observation for checking source detection.
§ Ogasawara station did not participate in the observation. The data are not used in the present paper.

and IDM99 (intensity-weighted velocity). However, the individual flux densities of the spectral peaks have varied, the whole spectrum, especially the number of the peaks, has not varied significantly within one year.

Table 1 gives the numbers of detected maser features in the individual epochs. The increase in the number of features at the fourth and fifth epochs was the result of better sensitivity, while that at the sixth epoch indicates possible intrinsic change in the maser source environment. Figure 4 shows a composite map of the IRC −10414 $H_2O$ masers, which was synthesized from the maser distributions at all epochs. The most blue-shifted maser features ($V_{\rm LSR} \sim 30\,{\rm km\,s^{-1}}$, ID 28, 29, 30, 32, 33, 34, hereafter denoted as feature group A) and the most red-shifted maser features ($V_{\rm LSR} \sim 55\,{\rm km\,s^{-1}}$, ID 1, 2, 3, hereafter denoted as feature group B) are located close to the center of the maser distribution. We note that the average velocity of groups A and B is $V_{\rm LSR} \approx 42.5\,{\rm km\,s^{-1}}$, quite consistent with the systemic velocity estimated by Blommaert, van Langevelde, and Michiels (1994) and IDM99. The maser distribution is elongated to 260 mas in the north–south direction, implying the existence of a bipolar outflow in this direction. We also note that groups A and B are clearly split perpendicularly to the major axis of the elongation of the whole maser distribution, and that the middle point of these maser components is close to the dynamical center of the whole outflow. Among a number of possible explanations for the spatio-kinematical structure of groups A and B, three models are here supposed: a bipolar expanding outflow with a small inclination with respect to the line of sight, a spherically expanding outflow with a small elongation along the these maser groups, or a rotating disk whose rotation axis is parallel to the elongation of the whole maser distribution.

In order to characterize the seen structure, we adopted an expanding thick shell model; the shell consists of several thin shells each of which satisfies an equation for the observed radial velocity and the projected distance from the star $(V, r)$, as follows:

$$\left(\frac{r}{r_{\rm shell}}\right)^2 + \left(\frac{V - V_{\rm sys}}{V_{\rm exp}}\right)^2 = 1, \quad (1)$$

where $r_{\rm shell}$ is the radius of the thin shell, $V_{\rm exp}$ the expansion velocity of the thin shell, $V_{\rm sys}$ the systemic velocity of IRC −10414. Figure 2 shows the projected distance–radial velocity diagram of the maser features. The location of the common dynamical center of the shells is still assumed to be located at the mean of the maser feature positions, or close to the most blue-shifted feature, but is re-estimated in the model fitting analysis, as mentioned in subsection 3.5. We find that most of the maser features are located between the inner and outer shells with radii of 40 mas [80 $(D/2.0\,{\rm kpc})$ AU] and 100 mas [200 $(D/2.0\,{\rm kpc})$ AU], and expansion velocities of $3.8\,{\rm km\,s^{-1}}$ and $13.8\,{\rm km\,s^{-1}}$, respectively, except for the maser features located at the northern (ID 26) and southern (ID 7, 8, 9) edges of the maser distribution, which are moving outwards faster, as mentioned in subsection 3.5.

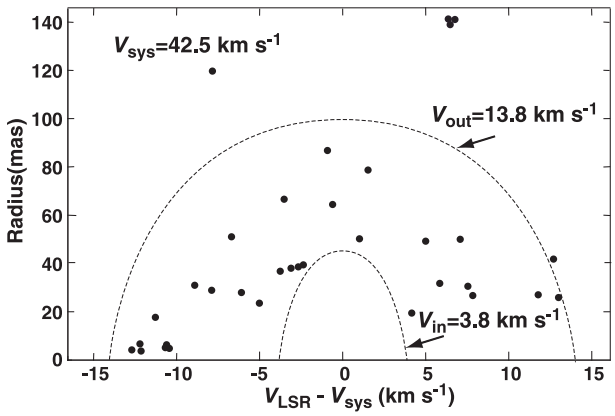


**Fig. 2.** Radial velocities of maser features relative to the systemic velocity ($V_{\rm sys} = 42.5\,{\rm km\,s^{-1}}$) against the projected distances from the flow dynamical center $(X, Y) \approx (0,0)$ [mas].

### 3.2. *3D Spatio-Kinematical Structure of the IRC −10414 Flow*

To elucidate the three-dimensional velocity field of $H_2O$ masers by obtaining the relative proper motions of the maser features, we identified the same maser features detected at the successive epochs, each of which was stable within 1 mas in position and $0.21\,{\rm km\,s^{-1}}$ in LSR velocity. Three maser features (ID 17, 23, and 27) were convincingly detected at all epochs, whose mean position was used as the coordinate reference to

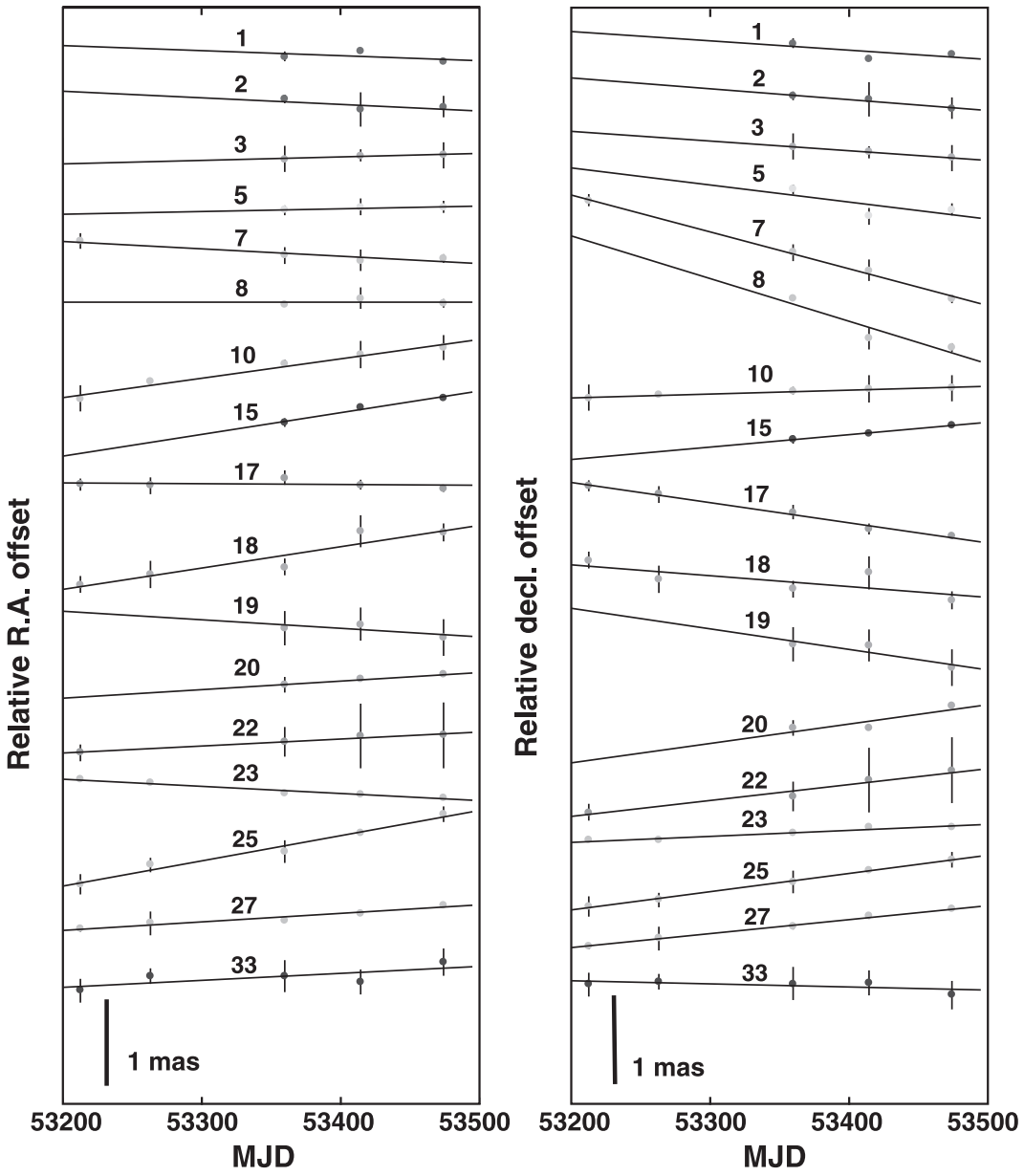


**Fig. 3.** Positions of maser features in RA (left panel) and Dec (right panel) against time (MJD). The straight solid line shows the relative maser feature proper motion, estimated by linear fitting.

register the maser maps for the proper motion measurement. The intrinsic motion of the coordinate reference, even if it is defined from a larger number of maser features as stable as the three, has some difference from the stellar motion. In the present paper, it is impossible to directly measure both motions. Instead, the relative value of the latter motion with respect to the former are can be indirectly estimated through an analysis of the three-dimensional kinematics of the maser features, as described in subsection 3.5. However, it still has some ambiguity, because none of the absolute coordinates of the maser features has been obtained, and possible biases in the spatial distribution and the kinematics would affect the estimated kinematical model.

Figure 3 shows the time variations of the positions of the maser features that were detected at least three times, and whose relative proper motions were measured. Table 2 summarizes the parameters of all $H_2O$ maser features detected in the present work. Their measured relative proper motions are also listed. The proper motions of 17 maser features were measured in the present work. Figure 4 shows the distribution and proper motions of all detected maser features. A bipolar outflow in the north–south direction is clearly recognized. In this direction, a proper motion of 1.77 mas yr$^{-1}$ [$17(D/2.0\,\mathrm{kpc})\,\mathrm{km\,s^{-1}}$] was found for feature ID 8. At the same time, we note that the proper motions of groups A and B are not very fast, which is consistent with the suggestion that they are either rotating around each other in the east–west direction, or moving outwards close to the line of sight. Because they

**Table 2.** Parameters of $H_2O$ maser features in IRC −10414.

| ID* | LSR velocity | | Position at the first epoch | | | | log ($I_{\rm peak}$)‡ | Relative proper motion | | | |
|---|---|---|---|---|---|---|---|---|---|---|---|
| | $V_{\rm LSR}$ | $\Delta V$† | $X$ | $\sigma_X$ | $Y$ | $\sigma_Y$ | | $\mu_x$ | $\sigma_{\mu_x}$ | $\mu_y$ | $\sigma_{\mu_y}$ |
| | (km s$^{-1}$) | | (mas) | | (mas) | | | (mas yr$^{-1}$) | | (mas yr$^{-1}$) | |
| 1 | 55.50 | 0.32 | −25.841 | 0.021 | −1.263 | 0.049 | --111 | −0.213 | 0.346 | −0.385 | 0.424 |
| 2 | 55.21 | 0.32 | −27.199 | 0.013 | −31.768 | 0.112 | --112 | −0.272 | 0.276 | −0.449 | 0.118 |
| 3 | 54.28 | 0.49 | −27.021 | 0.013 | 0.039 | 0.142 | --112 | 0.137 | 0.075 | −0.406 | 0.010 |
| 4 | 50.34 | 0.21 | 24.501 | 0.092 | −10.693 | 0.057 | ----1 | | | | |
| 5 | 50.05 | 0.28 | −6.525 | 0.021 | −29.842 | 0.060 | --112 | 0.111 | 0.063 | −0.711 | 0.735 |
| 6 | 49.58 | 0.32 | 11.261 | 0.225 | 48.689 | 0.070 | ----2 | | | | |
| 7 | 49.27 | 0.29 | −20.494 | 0.013 | −139.495 | 0.037 | 2-222 | −0.306 | 0.081 | −1.535 | 0.073 |
| 8 | 48.87 | 0.35 | −18.803 | 0.024 | −139.981 | 0.040 | --222 | −0.002 | 0.242 | −1.771 | 0.731 |
| 9 | 48.98 | 0.21 | −22.459 | 0.030 | −137.086 | 0.060 | --1-2 | | | | |
| 10 | 48.35 | 0.40 | 31.068 | 0.205 | 6.416 | 0.138 | 22222 | 0.801 | 0.075 | 0.162 | 0.016 |
| 11 | 47.50 | 0.11 | −9.709 | 0.060 | −48.266 | 0.060 | ----1 | | | | |
| 12 | 46.66 | 0.11 | 13.791 | 0.040 | −13.716 | 0.070 | ----1 | | | | |
| 13 | 44.03 | 0.21 | 17.855 | 0.078 | 76.628 | 0.035 | ----1 | | | | |
| 14 | 43.52 | 0.32 | −41.949 | 0.092 | −27.615 | 0.091 | ----1 | | | | |
| 15 | 41.90 | 0.39 | 49.846 | 0.100 | 40.782 | 0.039 | --122 | 0.900 | 0.133 | 0.517 | 0.039 |
| 16 | 41.59 | 0.32 | 10.969 | 0.056 | 86.059 | 0.081 | ----2 | | | | |
| 17 | 40.14 | 0.40 | −7.055 | 0.033 | −38.760 | 0.021 | 22222 | −0.040 | 0.086 | −0.839 | 0.052 |
| 18 | 39.83 | 0.34 | −4.980 | 0.024 | −38.271 | 0.091 | 22222 | 0.892 | 0.194 | −0.454 | 0.228 |
| 19 | 39.39 | 0.28 | −4.593 | 0.359 | −37.714 | 0.201 | --222 | −0.354 | 0.363 | −0.859 | 0.401 |
| 20 | 38.98 | 0.25 | 8.459 | 0.035 | 66.043 | 0.078 | --112 | 0.355 | 0.012 | 0.816 | 0.413 |
| 21 | 38.74 | 0.42 | −3.073 | 0.073 | −36.642 | 0.116 | ----2 | | | | |
| 22 | 37.49 | 0.63 | −4.310 | 0.167 | 23.135 | 0.366 | 2-222 | 0.298 | 0.037 | 0.671 | 0.104 |
| 23 | 36.41 | 0.63 | −18.379 | 0.144 | 21.067 | 0.016 | 32223 | −0.301 | 0.036 | 0.249 | 0.029 |
| 24 | 35.81 | 0.16 | −13.514 | 0.035 | −49.195 | 0.085 | ---11 | | | | |
| 25 | 34.62 | 0.61 | 21.937 | 0.103 | 18.787 | 0.109 | 21223 | 1.050 | 0.096 | 0.763 | 0.028 |
| 26 | 34.66 | 0.21 | 7.816 | 0.014 | 119.398 | 0.099 | --2-- | | | | |
| 27 | 33.60 | 0.61 | 25.434 | 0.026 | 17.693 | 0.012 | 22223 | 0.341 | 0.052 | 0.590 | 0.028 |
| 28 | 32.07 | 0.26 | 0.778 | 0.129 | −4.742 | 0.078 | ---12 | | | | |
| 29 | 31.90 | 0.32 | −1.104 | 0.025 | −6.211 | 0.015 | ----2 | | | | |
| 30 | 31.83 | 0.32 | 1.002 | 0.069 | −5.025 | 0.107 | ----2 | | | | |
| 31 | 31.22 | 0.32 | 15.153 | 0.026 | −9.118 | 0.012 | ----2 | | | | |
| 32 | 30.37 | 0.21 | 0.856 | 0.141 | −3.633 | 0.148 | --2-- | | | | |
| 33 | 30.30 | 0.46 | 2.530 | 0.042 | −6.171 | 0.105 | 22223 | 0.299 | 0.158 | −0.139 | 0.093 |
| 34 | 29.81 | 0.11 | 1.261 | 0.030 | −4.026 | 0.040 | ----2 | | | | |

* Spot ID number.
† Half velocity width.
‡ Logarithm of peak intensity, '−' for negative detection.

are slowly separating from each other, the latter case is our preferred interpretation.

### 3.3. Parallax Distance to IRC −10414

In the present paper, the distance to IRC −10414 can be directly estimated by both statistical treatment of parallax and model fitting to the spatio-kinematics of $H_2O$ masers. In the statistical treatment, it is assumed that the maser motions are isotropic, and distance $D$ is given in the following equation (Schneps et al. 1981):

$$D = \frac{1}{a_0}\frac{\sigma_V}{\sigma'_\mu} = \frac{\sigma_V}{a_0\sqrt{\sigma_\mu^2 - \epsilon_\mu^2}}, \quad (2)$$

$$\frac{\sigma_D}{D} = \left\{\frac{1}{2N} + \frac{1}{4N}\left[1 - \left(\frac{\sigma_\mu}{\epsilon_\mu}\right)^2\right]^{-1}\right\}^{1/2}, \quad (3)$$

where $a_0 = 4.74\,{\rm km\,s^{-1}mas^{-1}yr\ kpc^{-1}}$ is a conversion factor from a proper motion to a velocity, $N$ the number of maser features used in the calculation, $\sigma_V$ the standard deviation of the maser motions in the line of sight with respect to the estimated systemic velocity, $V_{\rm LSR} \approx 42.5\,{\rm km\,s^{-1}}$, $\sigma_\mu$ the standard deviation of the proper motion in either the RA or Dec direction. As shown in equation (2), any underestimation of the distance due to errors in the proper motion measurements, $\epsilon_\mu$, is corrected. The final distance value was obtained from the accuracy-weighted mean of the distance values obtained from the proper motions in the RA and Dec directions.

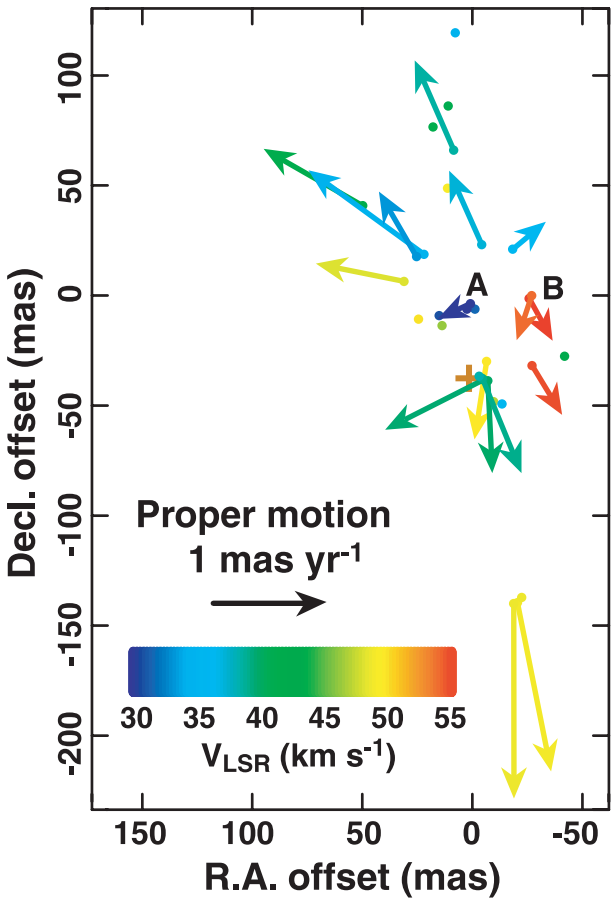


**Fig. 4.** Composite map and proper motion distribution of the IRC −10414 $H_2O$ masers. The map origin is located at the position of the reference maser spot at $V_{LSR} = 36.3\,km\,s^{-1}$. In the map, all maser features detected at least once appear. The feature color indicates the LSR velocity shown in the color scale at the bottom, which ranges from $29.8\,km\,s^{-1}$ to $55.5\,km\,s^{-1}$. An arrow indicates the location and the relative proper-motion vector of a maser feature, whose location is put where it was finally detected. The brown plus indicates the location of the dynamical center of the isotropic expansion flow model (model1, see the main text). The locations of the maser feature groups A and B, which include the most blue-shifted and red-shifted features, are also indicated.

Table 3 gives the results of distance estimations using this method. The assumption of an isotropic velocity field of the masers may be valid in cases (iii) and (iv), in which the maser features ID 7 and 8 are eliminated from the calculation because they are associated with a bipolar outflow, and have faster proper motions. In cases (ii) and (iv), the differences between the largest positive and negative values of the proper motions and the line-of-sight velocities are adopted instead of the standard deviations of the maser motions. All distances given in the four cases agree to within 0.9 kpc. We adopted this value as an error of the distance estimation. We thus obtained the distance to IRC −10414 to be $D = 2.7 \pm 0.9$ kpc (in the most reliable case). The estimated distance is much larger than that previously adopted (∼ 0.7 kpc: Jura & Kleinmann 1989). However, the model fitting results mentioned in subsection 3.5 support a larger distance. Note that the statistical parallax distance may be slightly overestimated due to a bias of the spatio-kinematical

**Table 3.** Derived parallax distances by the statistical treatment.

| Case | Feature selection | $N$ | Method | $\sigma_V$* | $\sigma_\mu$† | Distance (kpc) |
|---|---|---|---|---|---|---|
| i | All | 17 | RMS | 1.63 | 0.57 | $3.0 \pm 0.7$ |
| ii | All | 17 | PP | 5.30 | 2.07 | $\sim 1.8$ |
| iii | Center | 15 | RMS | 1.67 | 0.47 | $3.6 \pm 0.8$ |
| iv | Center | 15 | PP | 5.30 | 1.53 | $\sim 2.1$ |
| | | | Mean (i+ii+iii+iv) | | | $2.6 \pm 0.8$ |
| | | | Mean (iii+iv) | | | $2.7 \pm 0.9$ |

* Doppler velocity standard deviation in $km\,s^{-1}$.
† Proper motion standard deviation in mas $yr^{-1}$.

distribution of the maser features, as mentioned in subsection 3.4. Since the following analysis and discussion, we adopt a distance value of 2.0 kpc, which is obtained in subsection 3.5, and is still consistent with that obtained in this section.

### 3.4. *Analysis of the Maser Spatio-Kinematics Based on the Variance–Covariance Matrixes*

To objectively analyze the maser kinematics, and to find the major axis of the bipolar outflow, we applied the velocity variance–covariance matrix (VVMC) diagonalization procedure (Bloemhof 2000). The VVCM consists of elements calculated from the velocity dispersions, as follows:

$$\sigma_{i,j} = \frac{1}{N-1}\sum_{n=1}^{N}(v_{i,n} - \overline{v}_i)(v_{j,n} - \overline{v}_j), \tag{4}$$

where $i$ and $j$ denote three orthogonal space axes (e.g., RA, Dec, and radial coordinate $z$), $n$ denotes the $n$-th maser feature in a collection totaling $N$, and the bar indicates averaging over the maser spots. The eigenvector giving the largest eigenvalue indicates the kinematical major axis of the outflow. For IRC −10414, the velocity VVCM is diagonalized as follows (in units of $km^2\,s^{-2}$):

$$\begin{pmatrix} 19.26 & 18.36 & -12.62 \\ 18.36 & 54.72 & -30.07 \\ -12.62 & -30.07 & 64.15 \end{pmatrix} \Rightarrow \begin{pmatrix} 11.47 & 0 & 0 \\ 0 & 30.70 & 0 \\ 0 & 0 & 95.95 \end{pmatrix}. \tag{5}$$

The largest eigenvalue has a larger value by a factor of three than the second-largest eigenvalue, and its corresponding eigenvector has an inclination of −44.°3 with respect to the celestial sphere and a position angle of 23.°0 east from north. Note that only the inclination of the eigenvector changes by ∼ 20°, depending on the adopted distance (2–3 kpc). Although the three eigenvalues have different values by a factor of about three, the velocity collimation is consistent with the spatial collimation along the eigenvector corresponding to the largest eigenvalue. If we adopt a much shorter distance to IRC −10414, the maser kinematical structure appears to be tri-axially asymmetric, in which the velocity vectors are more collimated in the line of sight.

### 3.5. *Model Fitting Analysis*

To analyze the spatio-kinematical structure of the maser features and to estimate the distance to IRC −10414 in another

**Table 4.** Parameters of the best-fit 3D spatio-kinematical models of the $H_2O$ masers.

| Parameter | Model 1 | Model 2 | Model 3 |
|---|---|---|---|
| **Offsets** | | | |
| Velocity: | | | |
| $V_{0x}$* (km s$^{-1}$) ..... | 1.5 ± 2.1 | 4.8 ± 0.6 | 5.7 ± 0.5 |
| $V_{0y}$* (km s$^{-1}$) ..... | −6.5 ± 2.9 | −5.8 ± 0.6 | −4.9 ± 0.6 |
| $V_{0z}$† (km s$^{-1}$) ..... | 42.5‡ | 39.8 ± 0.6 | 39.8 ± 0.5 |
| Position: | | | |
| $x_0$ ($''$) ..... | 0.000 ± 0.009 | 0.018 ± 0.006 | 0.022 ± 0.006 |
| $y_0$ ($''$) ..... | −0.037 ± 0.008 | −0.028 ± 0.006 | −0.025 ± 0.006 |
| **Velocity field** | | | |
| Radial outflow: | | | |
| $V_1$ (km s$^{-1}$arcsec$^{-\alpha}$) | ...§ | 24.9 ± 1.2 | 30.4 ± 1.5 |
| $\alpha$ ..... | ...§ | 0.25 ± 0.10 | 0.33 ± 0.10 |
| Rotation: | | | |
| $\omega_x$ (km s$^{-1}$arcsec$^{-1}$) | ... | ... | 6.2 ± 3.1 |
| $\omega_y$ (km s$^{-1}$arcsec$^{-1}$) | ... | ... | 6.2 ± 3.1 |
| $\omega_z$ (km s$^{-1}$arcsec$^{-1}$) | ... | ... | 0.3 ± 6.5 |
| Distance $d$ (kpc) .... | 3.0‖ | 2.03 ± 0.19 | 2.05 ± 0.18 |
| RMS residual $\sqrt{S^2}$ .. | 0.97 | 3.58 | 3.68 |

* Relative value with respect to the position-reference maser feature.
† Velocity with respect to the local standard of rest.
‡ Model 1 assumes the systemic radial velocity: $V_{0z} \equiv 42.5\,\mathrm{km\,s^{-1}}$.
§ The solution determines a radial outflow velocity $V_{\exp}(i)$ independently for each feature with a proper motion.
‖ Distance is completely covariant with the $z_i$ and $V_{\exp}(i)$ and cannot be determined: $d \equiv 3.0$ kpc.

independent way, we performed a model-fitting analysis, as applied by Imai et al. (2000) using the proper motion and the LSR velocity data (cf. Engels 1979). This procedure has only one critical assumption, namely that the direction of the velocity vector of the maser feature is close to the radial direction from the originating point of the expanding flow. This assumption may be valid for the IRC −10414 outflow, which exhibits radial expansion. Even if one includes rotation and other biased motions, such motions may be recognized as a deviation from the radial expansion.

The model fitting method relies on an estimation of the least-squares sum of the differences between the observed and model velocities, $S^2$:

$$S^2 = \frac{1}{3N_\mathrm{m} - N_\mathrm{p}} \sum_i \left\{ \frac{[\mu_{ix} - w_{ix}/(a_0 d)]^2}{\sigma_{ix}^2} + \frac{\left[\mu_{iy} - w_{iy}/(a_0 d)\right]^2}{\sigma_{iy}^2} + \frac{[u_{iz} - w_{iz}]^2}{\sigma_{iz}^2} \right\}, \quad (6)$$

where, $N_\mathrm{m}$ is the number of maser features with detected proper motions and $N_\mathrm{p}$ the number of free parameters in the model fitting; $a_0 = 4.74\,\mathrm{km\,s^{-1}\,mas^{-1}\,yr\,kpc^{-1}}$ is a conversion factor from proper motion to linear velocity; $d$ is the distance from the Sun to the maser feature cluster; $\mu_{ix}$ and $\mu_{iy}$ are the observed proper-motion components in the right ascension and declination directions, respectively and $u_{iz}$ is the observed LSR velocity of the maser feature. Note that, in the present paper, the errors of the observed proper-motion vector ($\sigma_{ix}$, $\sigma_{iy}$) are purely equal to the measurement uncertainty, and do not contain any turbulence velocity (cf. Imai et al. 2000). The LSR velocity error, $\sigma_{iz}$, is set to be equal to the observed velocity width. The above equation contains terms depending on the three-dimensional positions of the detected maser features. Here, the position of a maser feature in the line of sight, $z_i$, which cannot be directly measured, is estimated as being a part of the free parameters by

$$z_i = \frac{(u_{iz} - v_{0z})(r_{ix}^2 + r_{iy}^2)}{(u_{ix} - v_{0x})r_{ix} + (u_{iy} - v_{0y})r_{iy}}. \quad (7)$$

Equation (7) satisfies the following constraint; (the obtained position makes the value $S^2$ smallest):

$$\frac{\partial S^2}{\partial z_i} = 0. \quad (8)$$

In the present paper, three velocity field models are attempted in turn for model fitting. In the first step (Model 1), only a radially expanding motion is included, in which the expanding velocities are independently calculated for the individual maser features. The expansion velocity for the $i$-th maser feature, $V_{\exp}(i)$, is approximated by

$$V_{\exp}(i) = \frac{(u_{ix} - v_{0x})r_{ix} + (u_{iy} - v_{0y})r_{iy} + (u_{iz} - v_{0z})r_{iz}}{r_i}, \quad (9)$$

where

$$u_{ix} = \mu_{ix} a_0 d, \;\; u_{iy} = \mu_{iy} a_0 d, \quad (10)$$

$$r_{ix} = x_i - x_0, \quad r_{iy} = y_i - y_0, \quad r_{iz} = z_i. \tag{11}$$

Here, equation (9) must also satisfy the constraint shown in equation (8). In the second step (Model 2), the model velocity vector, $\boldsymbol{w}_i(w_{ix}, w_{iy}, w_{iz})$, is given as a function of the maser position vector, $\boldsymbol{r}_i = \boldsymbol{x}_i - \boldsymbol{x}_0$, as

$$\boldsymbol{w}_i = \boldsymbol{V}_0 + V_{\rm exp}(i)\frac{\boldsymbol{r}_i}{r_i}, \quad V_{\rm exp}(i) = V_1 r_i^{\alpha}. \tag{12}$$

Here, $\boldsymbol{V}_0\,(v_{0x}, v_{0y}, v_{0z})$ is the systemic velocity vector of the outflow, $\boldsymbol{x}_0(x_0, y_0, 0)$ the position vector of the originating point of the outflow with respect to the motion of the position-reference maser feature, $\boldsymbol{x}_i(x_i, y_i, z_i)$ the observed position of the maser feature on the celestial sphere, $V_1$ a constant value that indicates the expansion speed of the flow at one arcsecond away from the flow origin, and $\alpha$ the power-law index of the flow speed. In this step, the systemic LSR velocity and the distance to IRC −10414 are also estimated as free parameters. In the third step (Model 3), a solid rotation of the flow around the flow major axis is also assumed, in which the model velocity vector is given as

$$\boldsymbol{w}_i = \boldsymbol{V}_0 + V_{\rm exp}(i)\frac{\boldsymbol{r}_i}{r_i} + \boldsymbol{\omega} \times \boldsymbol{r}_i. \tag{13}$$

The best parameter sets to minimize the value $S^2$ were calculated using the Levenburg–Marquart minimization technique. Table 4 summarizes the fitting results. Because $S^2$ is not much improved between Model 2 and Model 3, no rotation in the flow can be recognized. In fact, the rotation vector, $\boldsymbol{\omega}$, is not estimated with any significant accuracy. Model 2 may also have a problem, in which $\sqrt{S^2}$ is not reduced from that in Model 1, even if the number of free parameters increases. In Models 2 and 3, the estimated location of the dynamical center is significantly deviated from that which we originally estimated by eye, near the middle point between the most blue-shifted (group A) and red-shifted (group B) components. This may be attributed to the whole maser distribution, including the bipolar outflow elongated in the north–south direction, especially to the southern two maser features moving southward. We find $V_{\rm exp} \simeq 8\,{\rm km\,s^{-1}}$ near the flow origin ($\sim 30$ mas) and $V_{\rm exp} \simeq 17\,{\rm km\,s^{-1}}$ at the outer edge of the flow ($\sim 150$ mas). These values are still roughly equal to those found in typical circumstellar envelopes of AGB stars, although the IRC −10414 outflow has high collimation in the maser distribution and velocity field. The distance to IRC −10414 is estimated to be $2.0 \pm 0.2$ kpc, which is smaller than, but consistent with, that estimated in the statistical parallax method (see subsection 3.3) and much larger than that previously adopted (710 pc: Jura & Kleinmann 1989).

## 4. Discussion

### 4.1. A Bipolar Slow Outflow in IRC −10414

To unambiguously elucidate the spatio-kinematical structure of $H_2O$ masers in IRC −101414, we estimated the three-dimensional structure of the maser spatio-kinematics by calculating each of the maser feature positions along the line of sight, $z_i$ [equation (7)]. Figure 5 represents three-dimensional views of the maser spatio-kinematics when assuming that the origin of the outflow is located at the middle point between maser groups A and B, and that the systemic velocity vector, or the velocity vector of the flow driving source, is (0.0, 0.0, 42.5) [km s$^{-1}$]. This model can naturally explain the radial expansion with a less collimated bipolar outflow, whose major axis is consistent with the eigenvector corresponding to the maximum eigenvalue described in subsection 3.4. However, we could not find any reasonable converging solution in the model fitting for this case.

Figure 6 is the same as figure 5, but the distance to

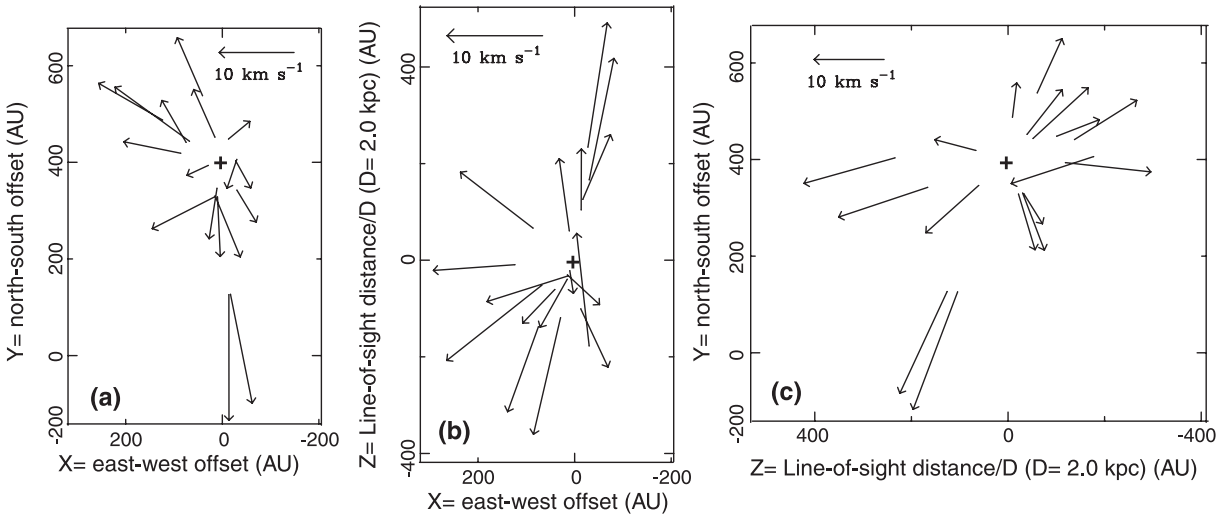


**Fig. 5.** Estimated three-dimensional positions and motions of $H_2O$ maser features in IRC −10414. The feature position was measured with respect to the originating point of the outflow, which is assumed to be located at the middle point between feature groups A and B (plus), and indicated by the position of the arrow. The feature motion vector is expressed in equation (7). Here, the distance to IRC −10414 is adopted to be 2.0 kpc. The direction and the length of the arrow show the direction and magnitude of the proper motion, respectively. (a) Front view ($XY$-plane) of the proper motions. (b) Top view ($XZ$-plane) of the proper motions. (c) East-side view ($YZ$-plane) of the proper motions.

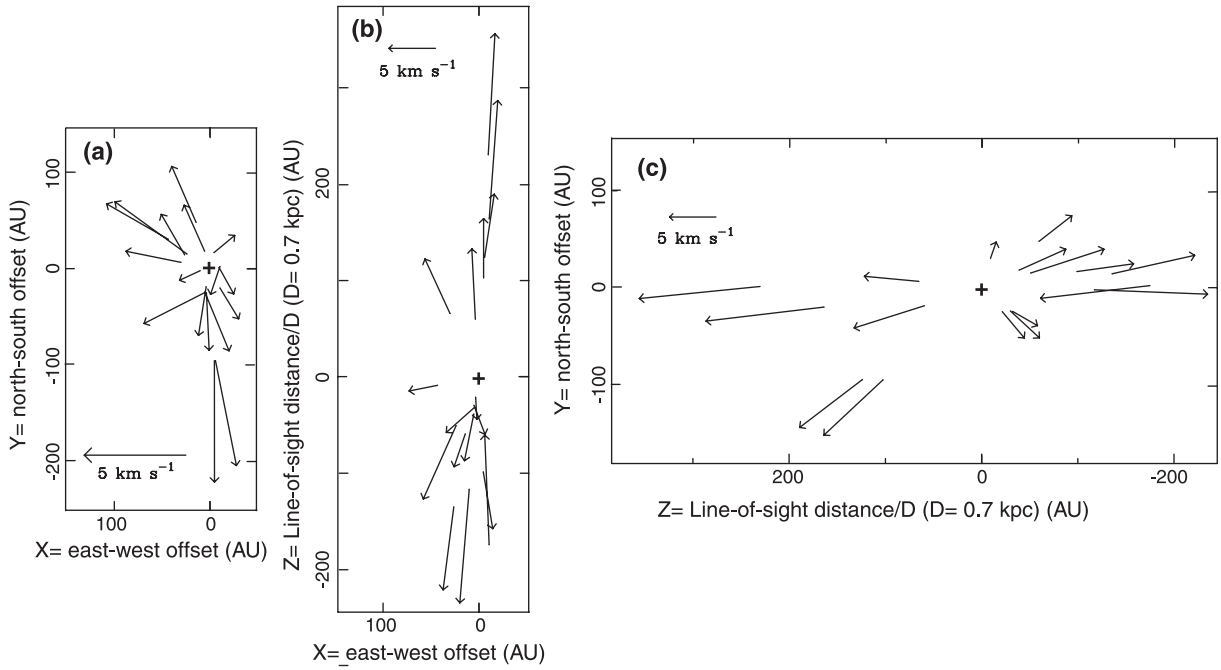


**Fig. 6.** Same as figure 5, but the distance to IRC −10414 is assumed to be 700 pc.

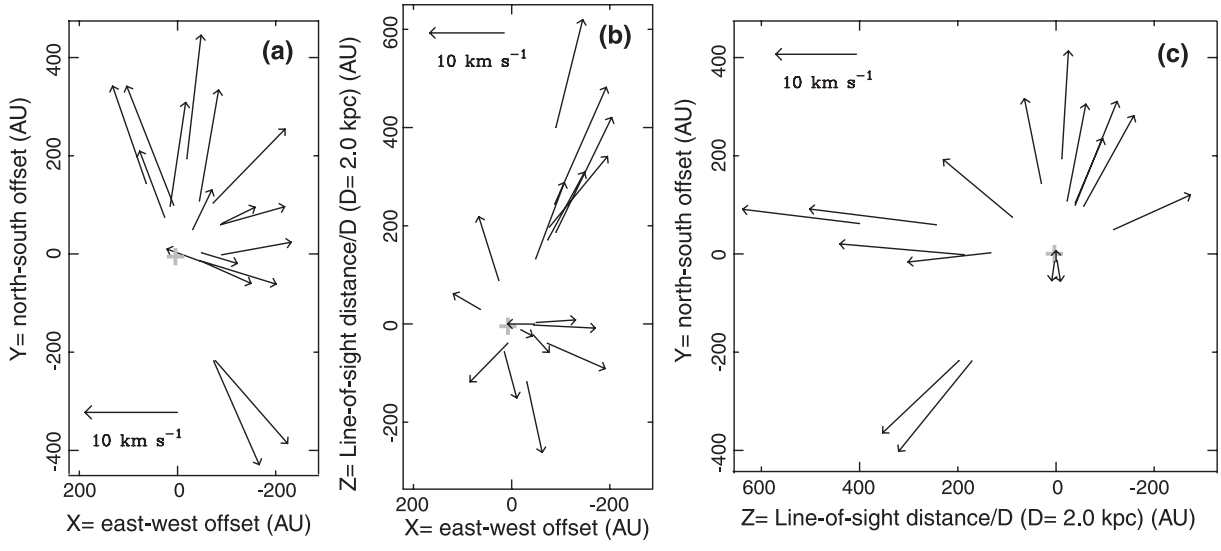


**Fig. 7.** Same as figure 5, but the positions and the motions are with respect to those of the originating point of the outflow, which are estimated in Model 2 (gray plus).

IRC −10414 is assumed to be 700 pc. In this model, very high collimation in the maser distribution and velocity field is found in a bipolar outflow with a velocity of only 10 km s$^{-1}$. This model cannot be accepted, as discussed later. Figure 7 also represents three-dimensional views of the maser spatio-kinematics, but adopting the parameters obtained in Model 2. Although the maser distribution on the sky is biased with respect to the estimated origin of the outflow, the model can still naturally explain the radial expansion in a manner similar to the model shown in figure 5.

Thus, a bipolar outflow in the spatio-kinematical structure of $H_2O$ masers is clearly seen in IRC −10414. The direction, speed, and collimation degree of the bipolar outflow derived in the model fitting, however, depend mainly on the assumed distance to IRC −10414. If the distance is assumed to be 700 pc, as previously adopted (Jura & Kleinmann 1989), the direction of the major axis is almost pole-on (see figure 6). In the present paradigm of stellar mass loss from evolved stars, it is difficult to suggest the existence of highly collimated bipolar outflow with a slow ($V_{\rm exp} \lesssim 10$ km s$^{-1}$) speed.

All of the bipolar outflows observed from evolved stars with high collimation have high speeds ($V_{\rm exp} \geq 30\,{\rm km\,s^{-1}}$, e.g., Imai et al. 2002), at least faster than the expansion speeds of circumstellar envelopes traced by 1612 MHz OH maser emission (e.g., Elitzur 1992). Some $H_2O$ maser sources with intermediate expansion velocities ($V_{\rm exp} = 10$–$30\,{\rm km\,s^{-1}}$), especially in supergiants, are associated with bipolar outflows (e.g., Richards et al. 1996, 1998, 2004), but others are still associated with spherically expanding circumstellar envelopes ($V_{\rm exp} \lesssim 10\,{\rm km\,s^{-1}}$, e.g., Bowers et al. 1993; Bowers & Johnston 1994; Yates & Cohen 1994; Imai et al. 2003). Note that, in the latter case, a bipolar *fast* outflow may have just ignited and the spherical envelope will be drilled by the newly formed bipolar outflow (e.g., in WX Psc, Inomata et al. 2007). In such a source, $H_2O$ masers are still associated with the spherical envelope with a higher gas density, rather than with bipolar outflow that has a smaller density. There, the spherical envelope, itself, is also expanding with a velocity, of $V_{\rm exp} = 10$–$20\,{\rm km\,s^{-1}}$ (see also the case in VX Sgr, Murakawa et al. 2003). If the velocity of the collimated bipolar outflow is assumed to be smaller than $10\,{\rm km\,s^{-1}}$, the expansion velocity of the spherically expanding shell should be much smaller than $10\,{\rm km\,s^{-1}}$, or comparable to that of the circumstellar envelope traced by SiO maser emission ($2$–$3\,{\rm km\,s^{-1}}$) in order to recognize the collimation in the bipolar outflow. The possible expansion or random-motion velocity of the SiO maser envelope in IRC $-10414$, without any collimation, is estimated to be $V_{\rm exp} \gtrsim 5\,{\rm km\,s^{-1}}$ (Ueda et al. 2008), which is already comparable to the velocity of the collimated bipolar outflow in the low-velocity collimated flow model.

From figure 5c or 7c, it is expected that the bipolar outflow has a wide opening angle (a full width of $\sim 50°$), so that both features of groups A and B and the southern maser features are contained in the same bipolar (more likely biconical) outflow. This case similar to that in WX Psc, as mentioned above (Inomata et al. 2007).

We speculate that IRC $-10414$ may be in transition, and be in the process of developing a collimated outflow with a velocity much higher than $10\,{\rm km\,s^{-1}}$, similar to the so-called water fountain sources (e.g., Imai et al. 2002). To observationally recognize a collimated bipolar outflow, the flow velocity should be higher than $20\,{\rm km\,s^{-1}}$, which supports the larger value (2–3 kpc) of the distance to IRC $-10414$. The dynamical time scale of the IRC $-10414$ bipolar flow is estimated to be $\sim 70\,{\rm yr}$, which is comparable to those found in the water fountain sources (e.g., Imai et al. 2007).

### 4.2. A Rotating Disk in IRC −10414?

On the basis of an SiO maser observation, IDM99 proposed the existence of a rotating gas disk around the central star of IRC $-10414$. The axis of the proposed rotating disk is in the north–south direction, which is consistent with that of the major axis of the $H_2O$ maser outflow seen in the present results. However, the existence of the maser groups A and B (subsection 3.1) and the results of the model fitting analysis (subsection 3.5) strongly suggest that the systemic (stellar) LSR velocity should be 40–43 $\,{\rm km\,s^{-1}}$, which is inconsistent with that previously proposed ($34.1\,{\rm km\,s^{-1}}$: IDM99). Together with the discussion in subsection 4.1, the present results do not support the existence of a rotating disk on the scale of the $H_2O$ maser region. The spatio-kinematical structure of SiO masers in IRC $-10414$ is re-analyzed in Ueda et al. (2008) in more detail.

### 4.3. Classification of the Star IRC −10414

Previously, a distance of 710 pc to IRC $-10414$ (Jura & Kleinmann 1989) was adopted on the basis of an assumption that the stellar luminosity of IRC $-10414$ is $10000\,L_\odot$. Our estimated distance (2–3 kpc) gives a stellar luminosity of $(1$–$2) \times 10^5\,L_\odot$, forcing us to conclude that IRC $-10414$ should be a supergiant rather than a typical AGB star, which has a typical luminosity of 3000–$10000\,L_\odot$. The revised distance means that the distribution radius of the IRC $-10414$ $H_2O$ masers is 200–300 AU and the mass-loss rate is estimated to be $(3.3$–$7.2) \times 10^{-5}\,M_\odot\,{\rm yr^{-1}}$. It should be pointed out that AGB/post-AGB stars that harbor collimated outflows/jets may be luminous with extremely copious stellar mass loss, with rates of up to $10^{-3}\,M_\odot\,{\rm yr^{-1}}$ (Sahai et al. 2007). IRC $-10414$ is also expected to experience such a high mass-loss rate in its coming evolution. However, there still exists a missing link between the bipolar outflows with a wide opening angle, as can be seen in IRC $-10414$, and stellar jets with extremely high spatial and kinematical collimation, as seen in the "water fountain" sources. A larger sample of stellar bipolar outflows covering a wide range of the flow velocities would enable us to see a sequence of the evolution of stellar collimated jets.

## 5. Conclusions

The present VERA observations of $H_2O$ masers have revealed the three-dimensional spatio-kinematical structure in the AGB star IRC $-10414$. As suggested by previous SiO maser emission, which exhibited an anomaly in the flux ratio between $v = 1$ and $v = 2$ ($J = 1$–0) emission (IDM99), the circumstellar envelope of IRC $-10414$ has a complicated spatio-kinematical structure, including both a spherically expanding envelope and a weakly collimated bipolar outflow. Because the speed of the bipolar outflow is still slow ($\sim 15\,{\rm km\,s^{-1}}$), IRC $-10414$ is expected to be in transition from ignition of the jet to the development of a high velocity jet, as seen in water fountain sources. The distance to IRC $-10414$ was re-estimated to be 2–3 kpc, leading to a suggestion that the star is a supergiant with a luminosity of $1$–$2 \times 10^5\,L_\odot$ and a mass-loss rate of $3.3$–$7.2 \times 10^{-5}\,M_\odot\,{\rm yr^{-1}}$. Thus, the present paper supports the supposition that high-mass and intermediate-mass AGB stars, such as IRC $-10414$, may have evolved to the final stage of their life through the production of highly collimated fast-jets.

We acknowledge all staff members and students who have helped in array operation and in data correlation of the JVN/VERA. We deeply appreciate Dr. Philip J. Diamond for kindly checking our manuscript. T.O./H.I./S.K./H.K. and H.I. have been financially supported by a Grant-in-Aid for Scientific Research from Japan Society for Promotion Science (17340055 and 18740109/20540234, respectively).

## References


Aaquist, O. B., & Kwok, S. 1991, ApJ, 378, 599
Bloemhof, E. E. 2000, ApJ, 533, 893
Blommaert, J. A. D. L., van Langevelde, H. J., & Michiels, W. F. P. 1994, A&A, 287, 479
Bowers, P. F., Claussen, M. J., & Johnston, K. L. 1993, AJ, 105, 284
Bowers, P. F., & Johnston, K. J. 1994, ApJS, 92, 189
Cooke, B., & Elitzur, M. 1985, ApJ, 295, 175
Elitzur, M. 1992, Astronomical Masers (Dordrecht: Kluwer)
Engels, D. 1979, A&AS, 36, 337
Imai, H., et al. 2003, ApJ, 590, 460
Imai, H., Deguchi, S., & Miyoshi, M. 1999, PASJ, 51, 587 (IDM99)
Imai, H., Kameya, O., Sasao, T., Miyoshi, M., Deguchi, S., Horiuchi, S., & Asaki, Y. 2000, ApJ, 538, 751
Imai, H., Obara, K., Diamond, P. J., Omodaka, T., & Sasao, T. 2002, Nature, 417, 829
Imai, H., Sahai, R., & Morris, M. 2007, ApJ, 669, 424
Inomata, N., Imai, H., & Omodaka, T. 2007, PASJ, 59, 799
Jura, M., & Kleinmann, S. G. 1989, ApJ, 341, 359
Kleinmann, S. G., Dickinson, D. F., & Sargent, D. G. 1978, AJ, 83, 1206
Lada, C. J., Blitz, L., Reid, M. J., & Moran, J. M. 1981, ApJ, 243, 769
Lockwood, G. W. 1985, ApJS, 58, 167
Murakawa, K., Yates, J. A., Richards, A. M. S., & Cohen, R. J. 2003, MNRAS, 344, 1
Nordhaus, J., & Blackman, E. G. 2007, arXir:0707.3792
Richards, A. M. S., et al. 2004, in Proc. 7th European VLBI Network Symposium, ed. R. Bachiller, F. Colomer, J. F. Desmurs, & P. de Vicente, 209
Richards, A. M. S., Yates, J. A., & Cohen, R. J. 1996, MNRAS, 282, 665
Richards, A. M. S., Yates, J. A., & Cohen, R. J. 1998, MNRAS, 299, 319
Sahai, R., Morris, M., Sánchez Contreras, C., & Claussen, M. 2007, AJ, 134, 2200
Sahai, R., & Trauger, J. T. 1998, AJ, 116, 1357
Schneps, M. H., Lane, A. P., Downes, D., Moran, J. M., Genzel, R., & Reid, M. J. 1981, ApJ, 249, 124
Ueda, K., Imai, H., Maeda, T., Omodaka, T., & Kamohara, R. 2008, PASJ, 60, 1051
Ukita, N., & Goldsmith, P. F. 1984, A&A, 138, 194
Vlemmings, W. H. T., Diamond, P. J., & Imai, H. 2006, Nature, 440, 58
Yates, J. A., & Cohen, R. J. 1994, MNRAS, 270, 958